Chapter 5: Compositional Tests

Based on the results presented in the preceding chapters, it was decided that a study investigating the effect of compositional changes on corrosion of ferrous alloys in a molten salt mixture would be advantageous. It is stated by numerous sources that corrosion within a molten halide is due to selective leaching of chromium [1, 2]; this has been proven for stainless steel 316L by Zheng et al. [3], who witnessed chromium depletion along the grain boundaries in molten FLiBe at 700°C [3]. The elemental compositions of numerous different alloys were assessed and it was decided that two further alloys would be investigated, LDX2101 and 304L, to determine which elements aided in the formation of a corrosion layer. Plain iron was also included in this test campaign, and the compositions of each of the alloys are given in Table 5.1.

LDX2101 is a duplex stainless steel, with a microstructure which is a mixture of austenite and ferrite phases. It therefore showcases a combination of ferrite and austenite properties, one of which is enhanced corrosion resistance [4]. Stainless steel 304L was chosen as it is an austenitic phase like stainless steel 316L and still shows excellent corrosion resistance, but the chromium content is slightly higher than that of 316L [5]. Both LDX2101 and stainless steel 304L have higher chromium content compared to stainless steel 316L (18.31 wt. %, 21.42 wt. % and 16.36 wt. %, respectively). It is therefore intended that the effect of chromium content can be addressed in this work.

Table 5.1: Elemental compositions (wt. %) of stainless steel 304L, LDX2101 and iron, determined by ICP-OES and combustion methods by Element Materials Technology. The values for the elemental composition of iron were calculated by difference.

	Fe	Cr	Ni	Mn	Mo	Si	C	P	S
Stainless steel 304L	71.23	18.31	8.28	1.46	0.42	0.26	0.024	0.018	<0.003
LDX2101	71.20	21.42	1.55	4.69	0.21	0.68	0.021	0.013	<0.003
Iron	99.69	0.04	0.03	0.15	<0.01	0.02	0.03	0.01	0.022

The ratios of the major alloying additions iron, chromium, nickel, molybdenum and manganese are shown in Table 5.2.

Table 5.2: Approximate ratios of the major alloying elements in the three different steel samples.

	316L	304L	LDX2101
Fe:Cr	4.25:1	3.59:1	3.33:1
Fe:Ni	6.86:1	6.82:1	47.7:1
Fe:Mo	32.67:1	-	238.5:1
Fe:Mn	51.54:1	34.08:1	35.75:1
Cr:Ni	1.61:1	1.9:1	14.3:1
Cr:Mo	7.68:1	-	71.67:1
Cr:Mn	12.12:1	9.5:1	4.3:1
Ni:Mo	4.76:1	-	5:1
Ni:Mn	7.51:1	5:1	0.3:1
Mo:Mn	1.58:1	-	0.06:1

The visual results are shown in Figure 5.1, and it is evident that each sample has corroded in a different way. The iron samples show attack on the surface, as well as the formation of a well adhered black corrosion layer in both the one and three week tests. Stainless steel 304L shows the formation of a smooth grey corrosion layer, similar to the results obtained in the stainless steel 316L tests in Chapter 3. Finally, LDX2101 gives a dull grey corrosion product that does not cover the surface and is easily removed.

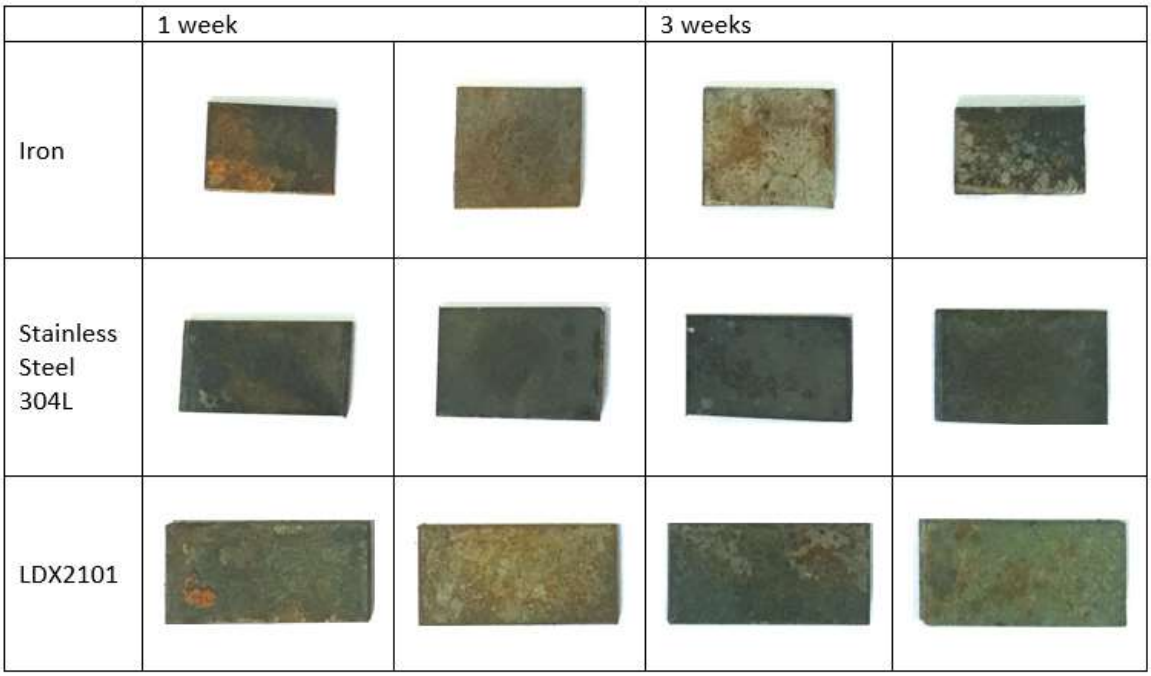

Figure 5.1: Samples after immersion in the molten salt for one and three weeks as marked, with duplicate coupons shown for each composition tested.

Further to visual analysis, the percentage mass change of each of the samples was also investigated. As previously stated, the measured mass loss accounts for both the mass loss due to corrosion, and the mass gain from corrosion product formation. Figure 5.2 shows the percentage mass change of the three new samples, along with the results from the repeated three week stainless steel test from Section 3.2 (Figure 3.9). Iron shows the highest percentage mass change, approximately -1% and -1.5% for the two samples, and LDX2101 shows the smallest, -0.1% and 0.0006%. This is expected as no alloying additions are present to prevent corrosion and leaching within the iron sample, and LDX2101 has the highest chromium content.

Although Figure 5.2 does suggest that LDX2101 is superior in resisting further corrosion, the visual analysis, Figure 5.1, suggests that LDX2101 forms a thick corrosion layer, which would result in a more substantial mass increase. In addition to this, the corrosion layer spalls very easily and therefore some of the corrosion layer will be lost before weighing the sample, which will result in a smaller percentage mass change. The analysis by SEM will give further insight into the level of protection offered by the LDX2101 corrosion layer. Stainless steel 304L has formed a uniform corrosion layer over the sample and from visual analysis alone, and it can be concluded that this gives the best protection against a molten salt within this experiment. The chromium content is slightly higher in stainless steel 304L compared to stainless steel 316L, and from Figure 5.1 and Figure 5.2 it appears that stainless steel 304L forms a similar protective layer over the bulk, (Figure 3.8) but with a lower % mass change.

From the % mass change alone it appears that as chromium content increases the % mass change decreases, but these results have to be assessed alongside the visual analysis, which suggests that the low % mass change could be due to the loss of the thick corrosion layer in LDX2101.

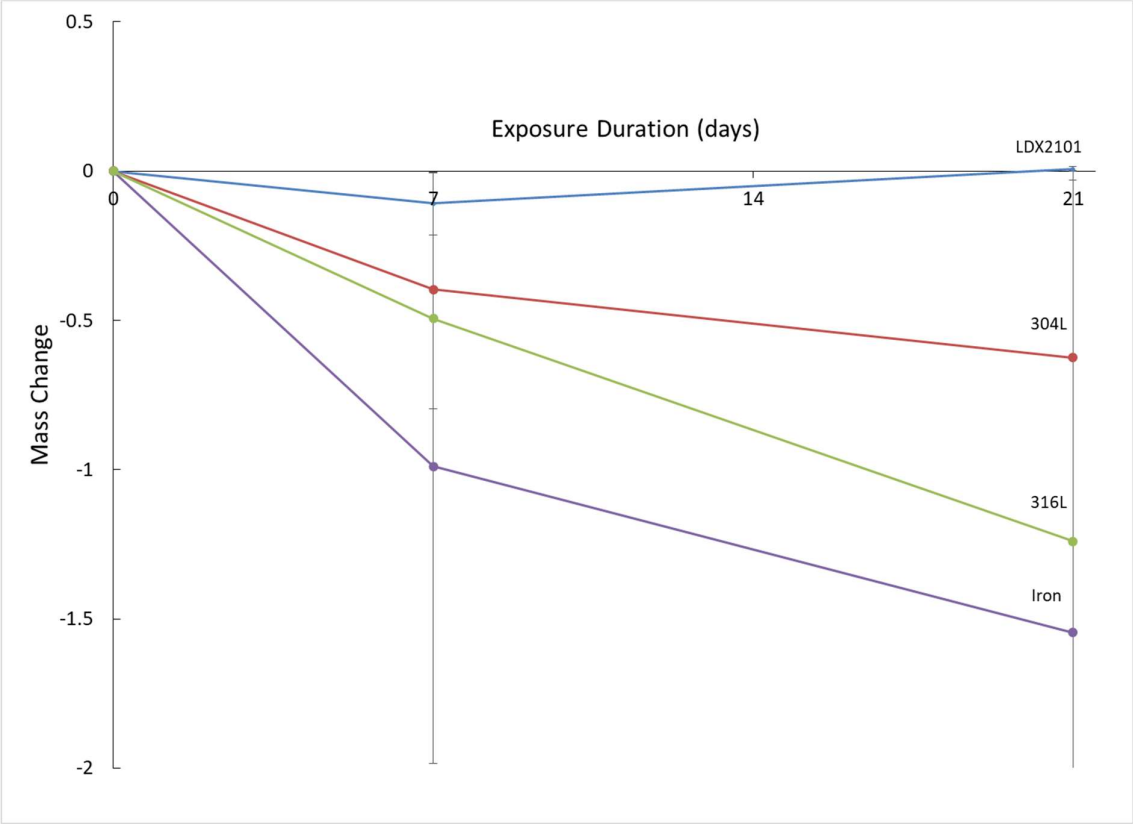

Figure 5.2: Mass change of the four different samples during corrosion as a percentage of initial coupon mass.

5.1: Stainless Steel 304L

5.1.1: XRD

The diffraction patterns for stainless steel 304L immersed for one and three weeks are shown in Figure 5.3, and follow the same trend as seen in Chapter 3. The diffraction pattern for the corrosion layer at three weeks shows a higher intensity compared to one week, this is expected due to the increased immersion time. Each of the diffraction patterns show peaks corresponding to stainless steel at approximately 44 and 51° 2θ. Some peak shift is evident and is due to the leaching of elements from the sample. Both patterns also show a peak at approximately 18° 2θ, due to the presence of a lithium spinel; this phase is believed to be lithium chromium oxide due to the broad double peak observed in both patterns between 63-64° 2θ, but this will be confirmed via EDX below. The stainless steel 304L shows a consistent result with no other oxides formed after three weeks according to the XRD data, which has previously been observed in the stainless steel 316L samples.

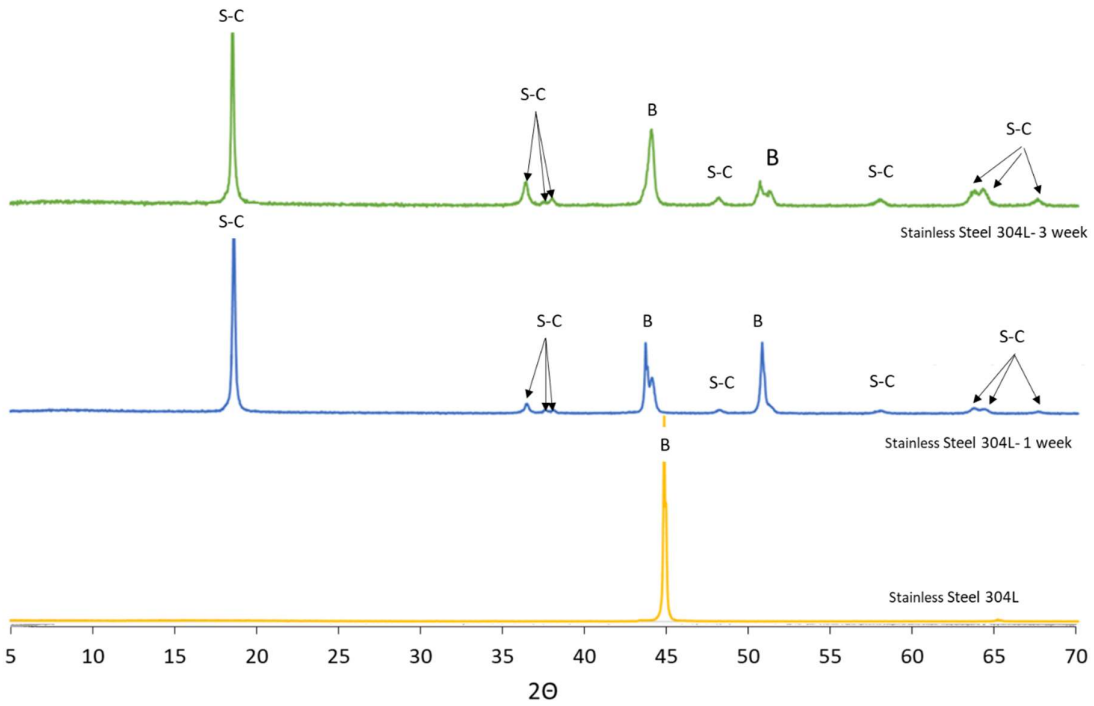

Figure 5.3: XRD patterns for the stainless steel 304L samples before immersion and after one and three weeks, where S-C corresponds to $LiCrO_2$ and B is for the bulk.

5.1.2 Surface and cross sectional SEM

The BSE images for stainless steel 304L are shown in Figure 5.4 and show consistent results, with a corrosion layer forming over the surface. It does appear that there is less surface coverage compared to stainless steel 316L, (Figure 3.11), and it is therefore suggested that a compositional difference between 304L and 316L could result in a reduced rate of chromium leaching.

The EDX analysis for the one week sample is shown in Figure 5.5 with a chromium oxide layer (ii) forming over the stainless steel bulk (i). This is comparable to results obtained in Chapter 3, if the three week tests are omitted.

As lithium compounds are clearly present within the diffraction pattern, this is believed to be the same corrosion product that has formed in Chapter 3, lithium chromium oxide.

Spot analysis was also conducted on region (ii) to further confirm the presence of chromium and oxygen and this is shown in Table 5.3 and shows clearly that chromium and oxygen are the major elements within the layer. The presence of iron is believed to be due to the bulk, as it was difficult to find locations where only the corrosion product could be analysed in the one week test sample.

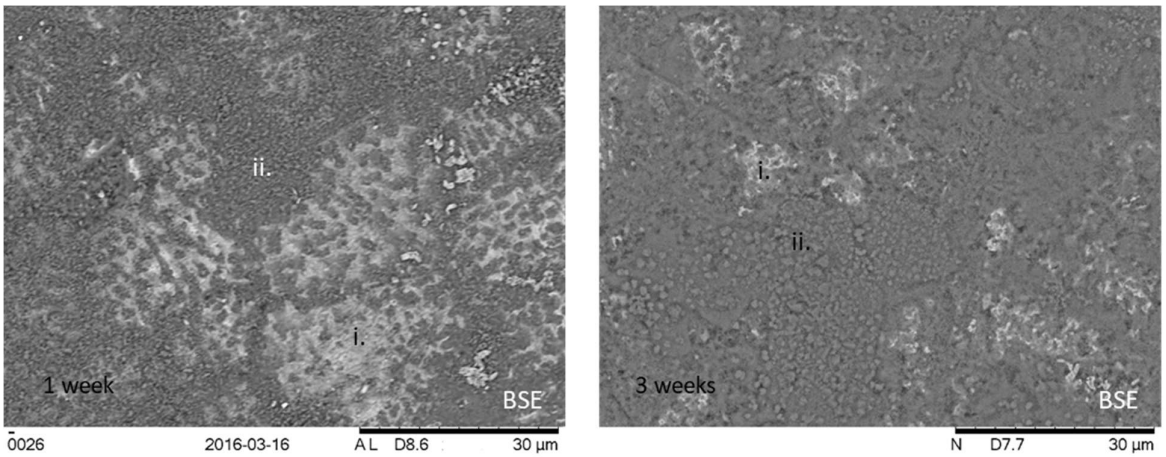

Figure 5.4: BSE images of stainless steel 304L held in a molten salt for a predetermined length of time (stated at the bottom left of each image).

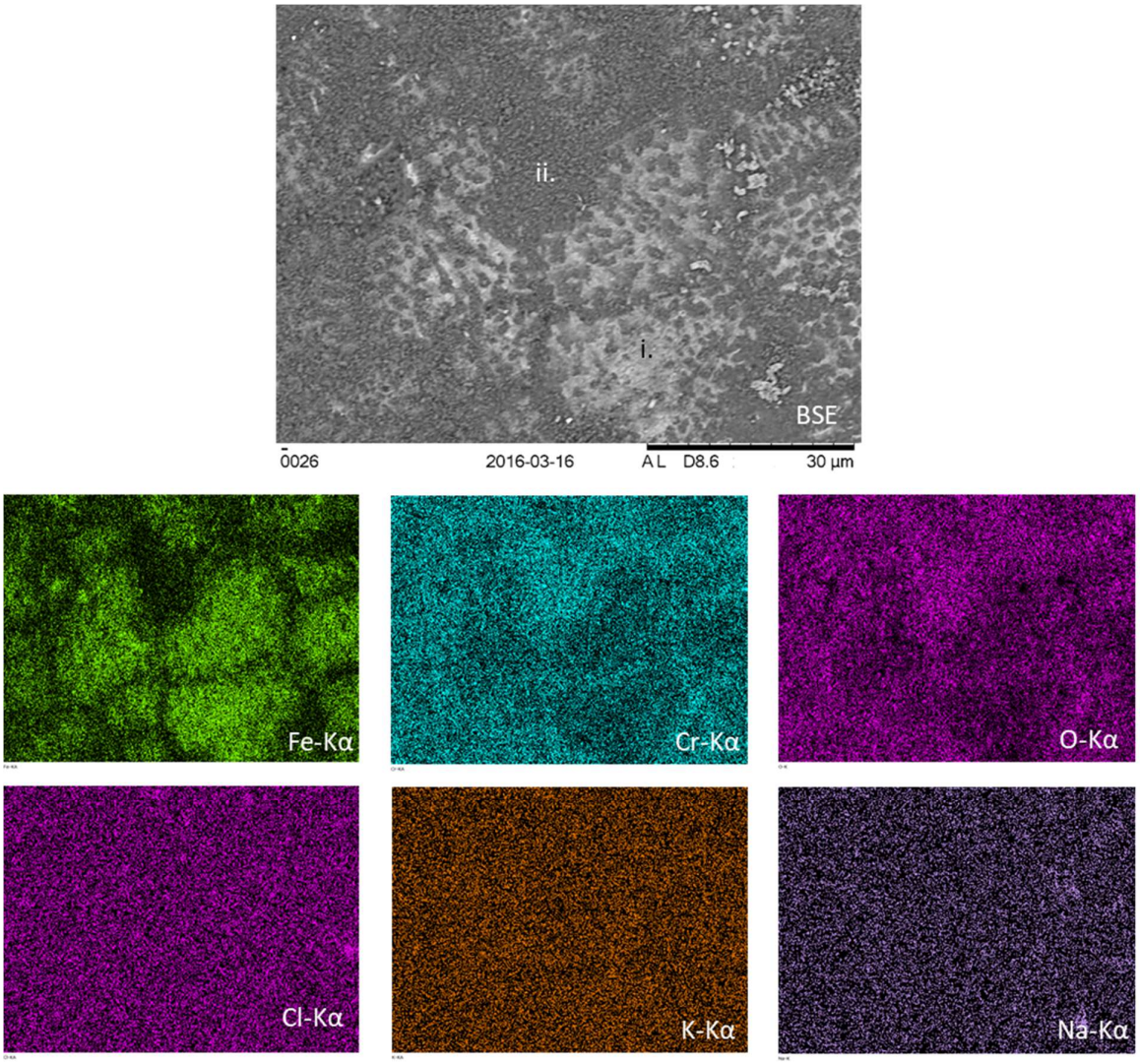

Figure 5.5: BSE image and corresponding EDX elemental maps for the surface of stainless steel 304L immersed in a molten alkali chloride eutectic for six weeks. Region (i) and (ii) are discussed in the text.

Table 5.3: Estimation of the elemental composition (at. %) of the area marked as (ii) in Figure 5.4.

Element	1 week test	3 week test
Chromium	49.1	58.1
Oxygen	39.6	41.9
Iron	7.5	
Carbon	3.1	
Chlorine	0.7	

The cross sectional SEM for the one and three week samples are shown in Figure 5.6, but give little information regarding the corrosion layer as it is too thin. One observation that can be made, is that it is clear that there has been no penetration into the bulk. Although these results are comparable to the stainless steel 316L tests, it was expected that due to the higher chromium content there would be better coverage by the corrosion layer. As it has not, it is highly likely that the formation of a corrosion product is dependent on more than just the chromium content. An investigation by Devan [6] in 1969, who investigated different alloying additions in nickel-molybdenum alloys, found that corrosion is enhanced when there is a higher wt. % of aluminium or titanium along with chromium in the alloy [6]. It is therefore possible that corrosion could be inhibited by the presence of certain elements in conjunction with chromium.

Stainless steel 304L does show a smaller percentage mass change compared to stainless steel 316L, but stainless steel 316L does appear to give a higher surface coverage to protect the bulk, and this could be responsible for the difference in % mass change. No anomalous results have been observed in stainless steel 304L, compared to stainless steel 316L where the three week tests (repeat) saw the formation of iron chloride and the initial three week sample formed numerous different oxides. However, work done by Malik et al. [7] in seawater at 50°C suggests that stainless steel 304L and stainless steel 316L, which they class as conventional stainless steels, behave in a similar fashion, so it is possible that the anomalous result that is seen at three weeks could also be seen in stainless steel 304L [7].

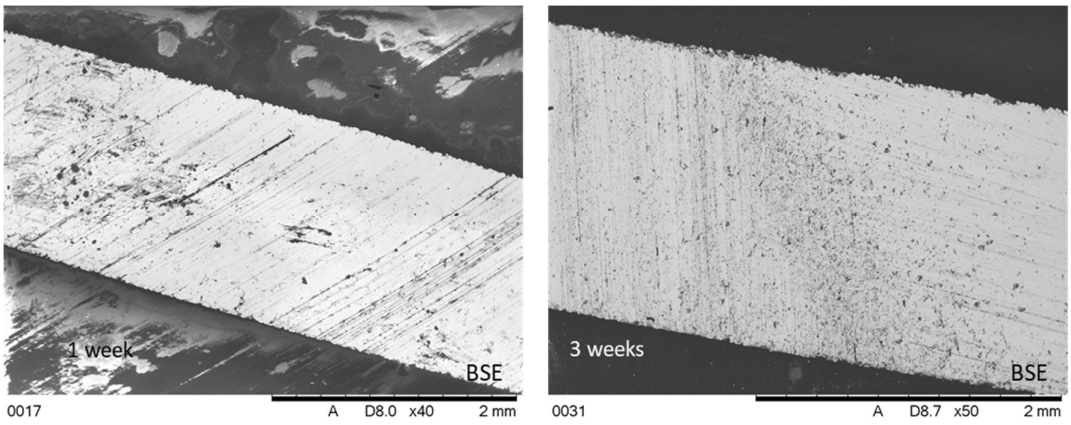

Figure 5.6: Cross sectional BSE images of stainless steel 304L held in a molten alkali chloride salt for a predetermined length of time (stated at the bottom left of each image).

5.2: LDX2101

5.2.1: XRD

The X-ray diffraction pattern for LDX2101 is shown in Figure 5.7 and shows similar results for both the one and three week tests, with the peaks corresponding to the bulk becoming less intense. Malik et al. [7] stated that stainless steel 304L and 316L will act in a similar manner, but as LDX2101 is a duplex stainless steel it is likely that it will behave differently and form different corrosion products. The XRD data are similar to the results obtained for previous tests, and it is likely that a lithium metal spinel has been formed. However, as stated in Chapter 3 (Figure 3.8), the diffraction patterns for lithium metal spinels are very similar and other products could be present. This will be examined further via SEM/EDX.

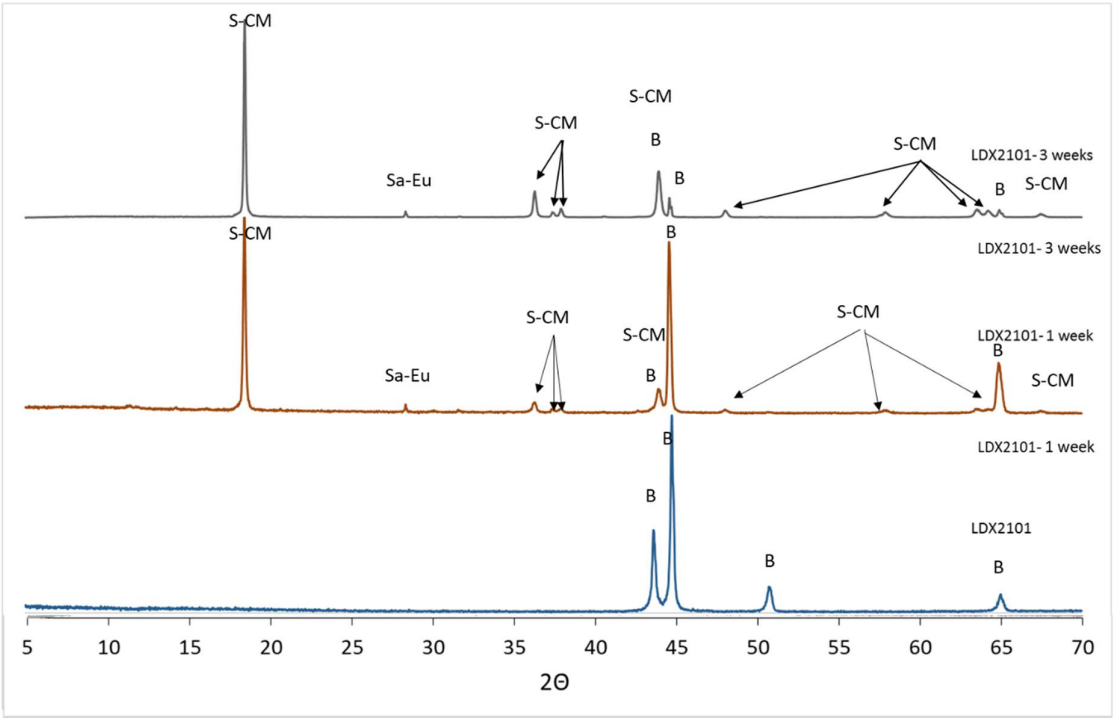

Figure 5.7: XRD patterns for the LDX2101 samples before immersion and after one and three weeks, where S-CM corresponds to a lithium spinel, Sa-Eu is for the eutectic salt and B is for the bulk.

5.2.2: Surface and Cross Sectional SEM

Results obtained for LDX2101 after immersion for one and three weeks are consistent with one another (Figure 5.8). In both the one and three week tests there is a thick corrosion layer (iii) and it does not cover the full surface. The corrosion product has not adhered well to the sample, which could explain the low percentage mass change observed in Figure 5.2, and it is possible that as immersion time increases the corrosion layer may become harder to remove. Low adhesion to the bulk has only been observed in the LDX2101 samples, which is unusual as it is stated that due to the greater thermal expansion coefficient of austenitic phases compared to ferritic there is a tendency for corrosion layers to spall in austenitic stainless steels [8]. Therefore, it is likely that kinetics plays a role in the spalling of the corrosion layer.

The EDX data are shown for the one week sample in Figure 5.9. The corrosion product (iii) observed in both the one and three week samples is made up of chromium and oxygen, this is confirmed via spot analysis, shown in Table 5.4. This was expected as the chromium content has increased by approximately 30% compared to stainless steel 316L, and has been reported by numerous authors investigating different structural alloys, such as Keiser et al. [9] and Shankar et al. [10] for stainless steels and Richardson et al. for Inconel, Monel and Hastelloy [11] that chromium will be preferentially leached from the bulk.

The structures of the crystals within the corrosion product are analogous to results obtained during the three week test in Chapter 3, where a blocky crystal has formed, but the presence of a blocky crystal tends to imply a lack of protection for the stainless steel bulk.

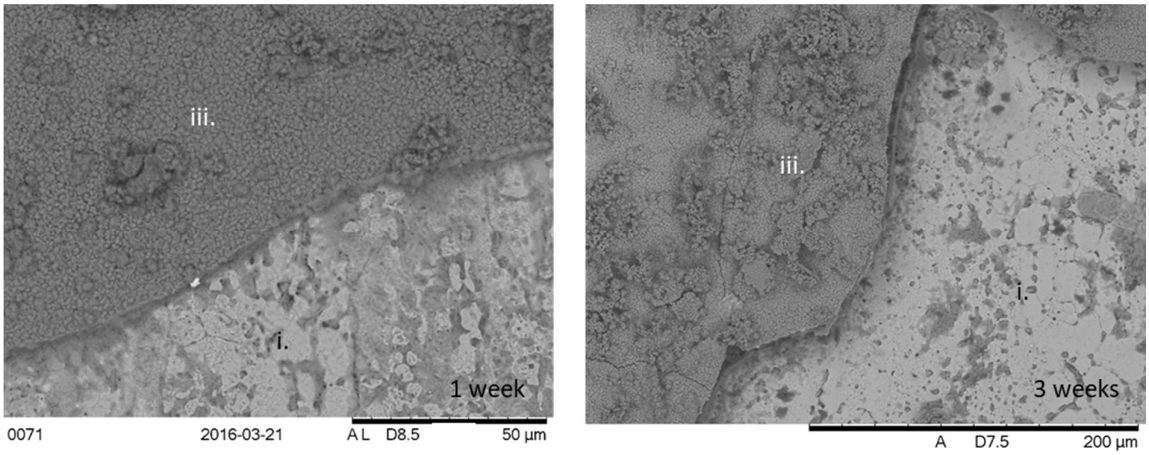

Figure 5.8: BSE images for LDX2101 in a molten chloride salt for a predetermined length of time (stated at the bottom right of each image).

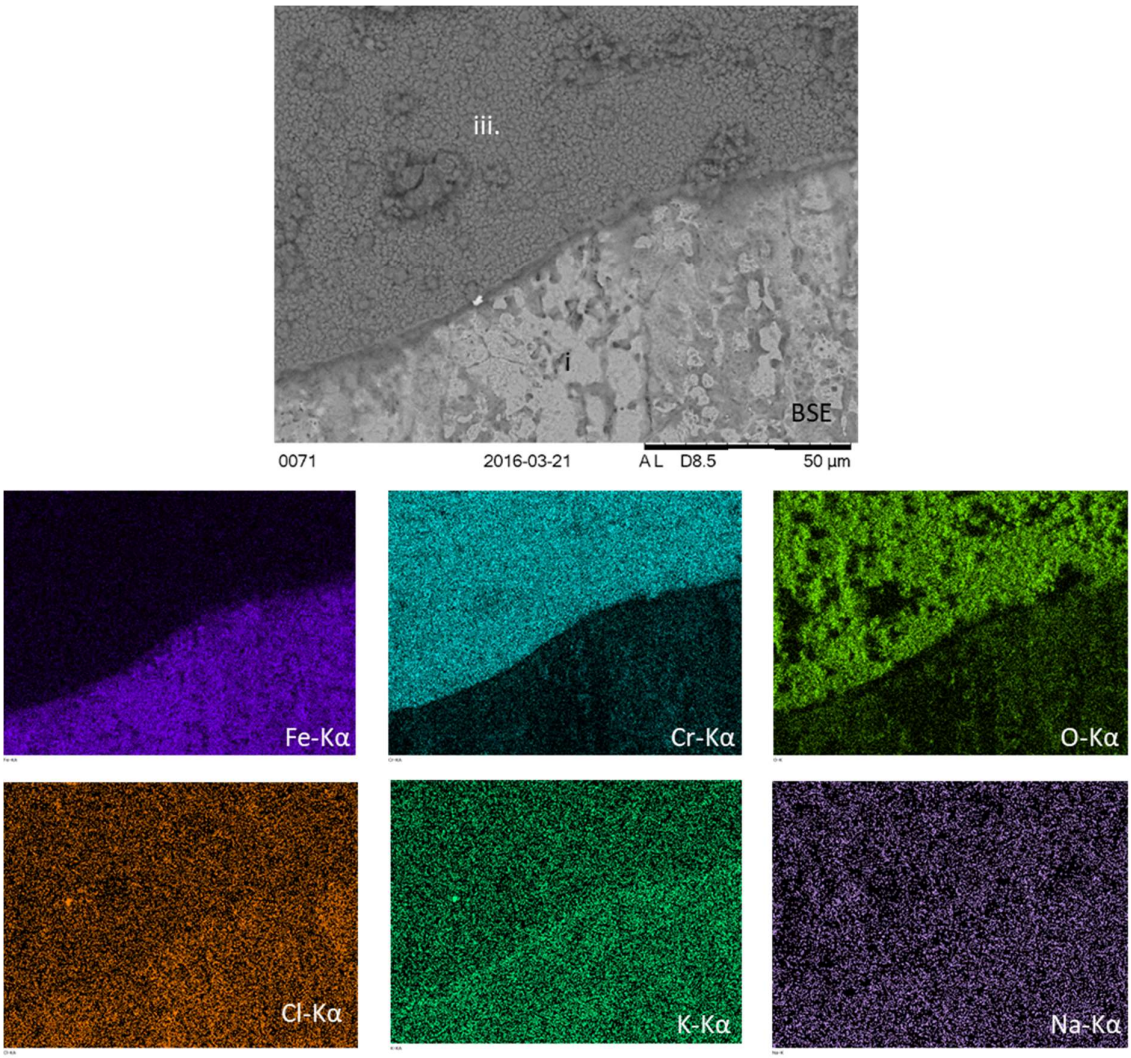

Figure 5.9: BSE image and corresponding EDX elemental maps for the surface of a LDX2101 coupon immersed in a molten chloride eutectic for one week. Regions (i) and (iii) are discussed in the text.

Table 5.4: Estimation of the elemental composition (at. %) of the area marked as (iii) in Figure 5.8.

Element	1 week	3 weeks
Chromium	64.24	82.67
Oxygen	34.96	17.33
Chlorine	0.8	

The cross sectional BSE images for one and three weeks are shown in Figure 5.10. The layer in the one week test gives little information as it is too thin; this has been seen continually throughout this work, but the three week test presents a different story and will be further examined using EDX in Figure 5.11.

The EDX analysis suggests that there is an inner layer made up of iron and oxygen (iv) with a thin chromium oxide layer over the top. The presence of a double corrosion layer, with an iron oxide diffusing into the bulk, has previously been seen in the six week stainless steel tests (Figure 3.15). It is believed that two corrosion products are formed: one which diffuses into the bulk, and is likely iron oxide (iv), and another containing chromium and oxygen, which forms on the surface and is lithium chromium oxide (iii).

As the inner iron oxide layer is not observable in the LDX2101 surface SEM analysis (Figure 5.8), the outer layer is clearly substantially thicker than the layer reported in the six week samples, (Figure 3.15) and this is likely due to the increased chromium content within the alloy. The presence of a double layer has previously been described by Sho et al., where after 72 hours a $LiFeO_2$ layer formed over Cr_2O_3 that had previously been formed on stainless steel 316L *[12].*

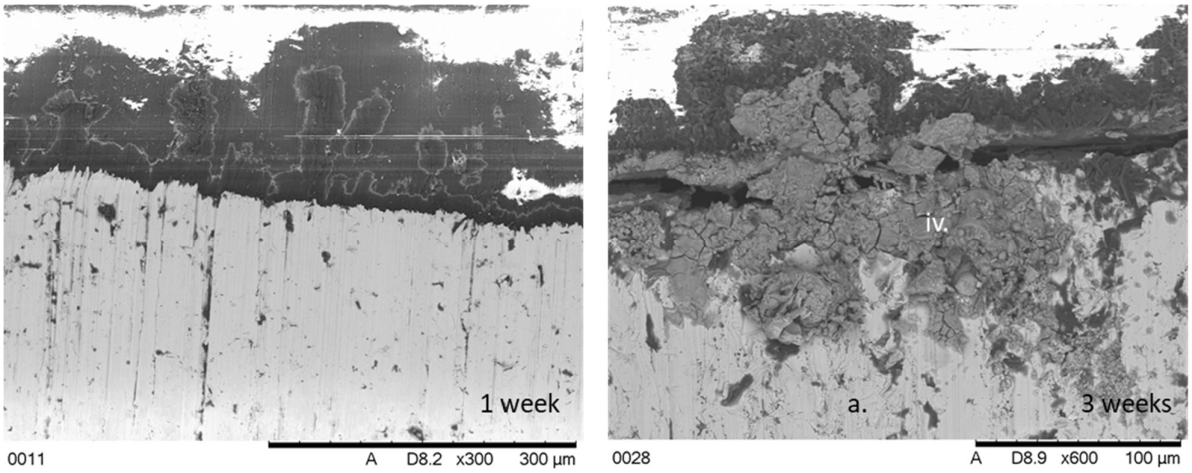

Figure 5.10: Cross-section BSE images of LDX2101 held in a molten chloride salt for a predetermined length of time (stated in the bottom right of each image).

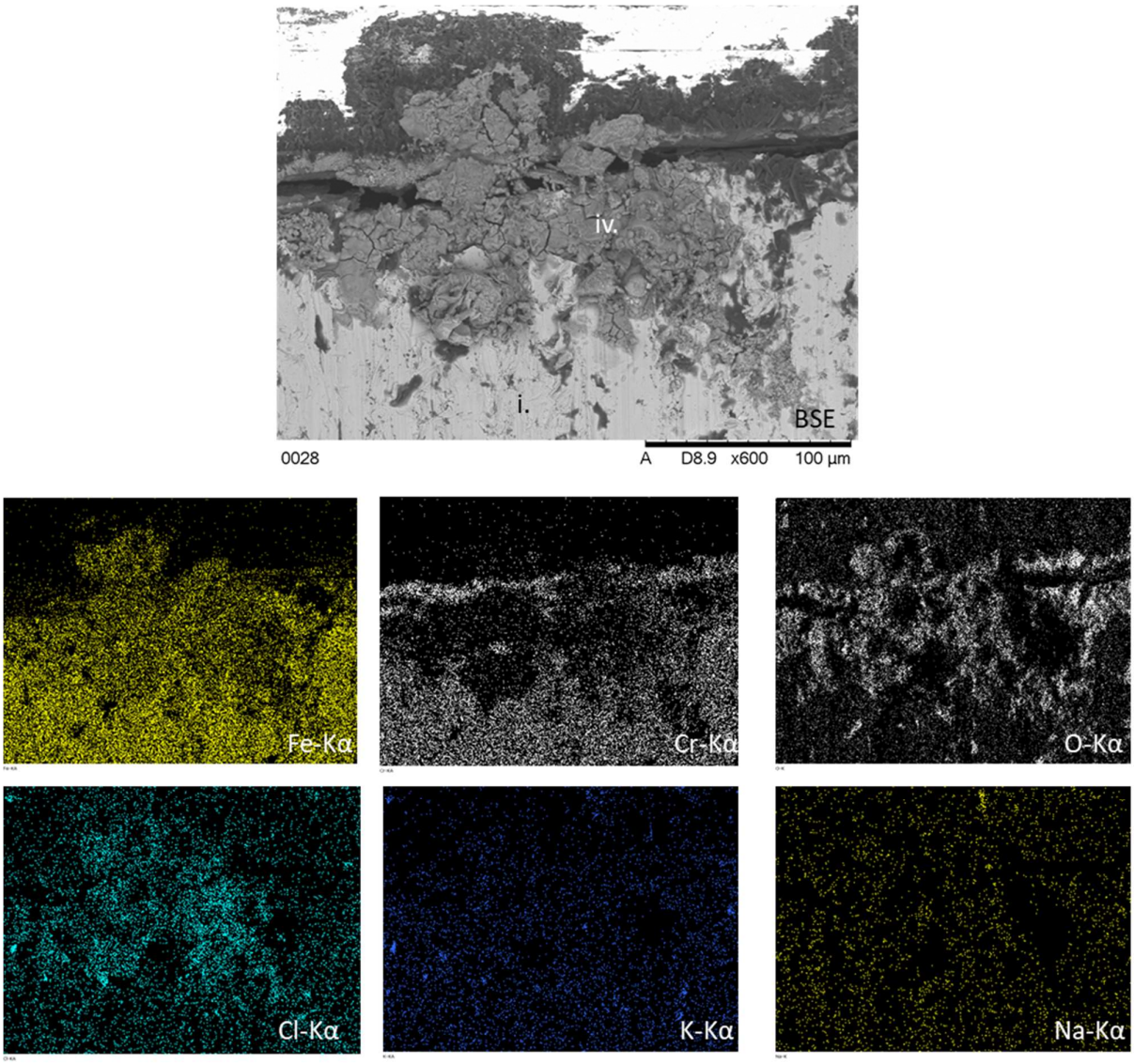

Figure 5.11: BSE and cross sectional EDX elemental maps for LDX2101 immersed in a molten chloride salt for three weeks.

5.3: Iron

5.3.1: XRD

Reiterating the results of the visual inspection of the tested iron samples, it is noticeable that the samples have resisted corrosion considerably well despite the lack of alloying additions. The XRD patterns for the one and three week iron tests (Figure 5.12) show the presence of iron oxide (Fe_3O_4) along with a strong iron peak. It is also possible that lithium iron oxide is present as this has a similar diffraction pattern to iron (II) oxide.

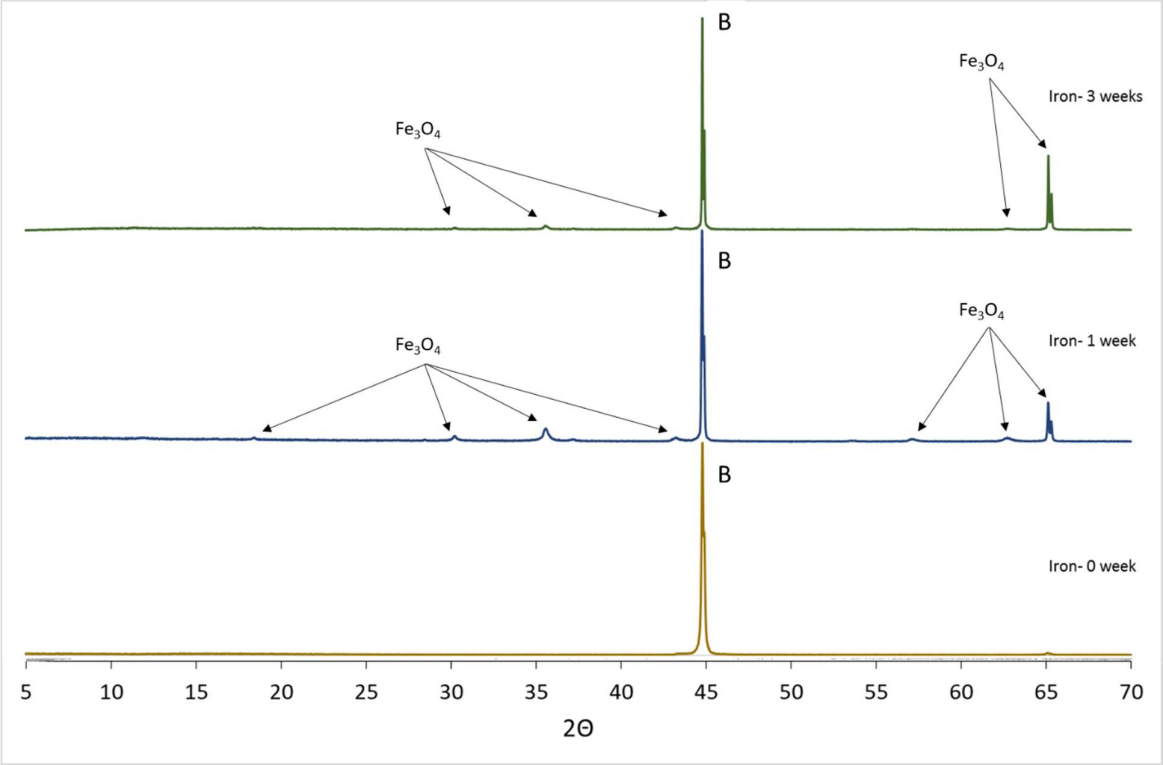

Figure 5.12: XRD patterns for the iron samples before immersion and after one and three weeks.

5.3.2: Surface and Cross Sectional SEM

Surface BSE images for iron after immersion for one and three weeks are shown in Figure 5.13. After one week of exposure the iron bulk (area (i)) is present along with area (v) which is relatively textured. The three week BSE image is different; there is a clear corrosion product there, but it is not as textured as the one week sample, therefore both sets of EDX data will be shown.

The EDX data for the one week test (Figure 5.14), suggested that iron, oxygen and possibly chloride are present in region (v), but with so few alloying additions iron is expected to leach and the identification of the anion it pairs with has proven difficult via the EDX data. The spot analysis shown in Table 5.5 has given further information and suggests that oxygen is the main anion for both corrosion products, but the different crystal structures do suggest two different compounds.

The surface EDX images for the three week test (Figure 5.15) suggest corrosion product (vi) is iron oxide. The iron bulk (i) appears different to the bulk that was initial observed in the one week test (Figure 5.13) therefore it is suggested that the iron surface has been attacked.

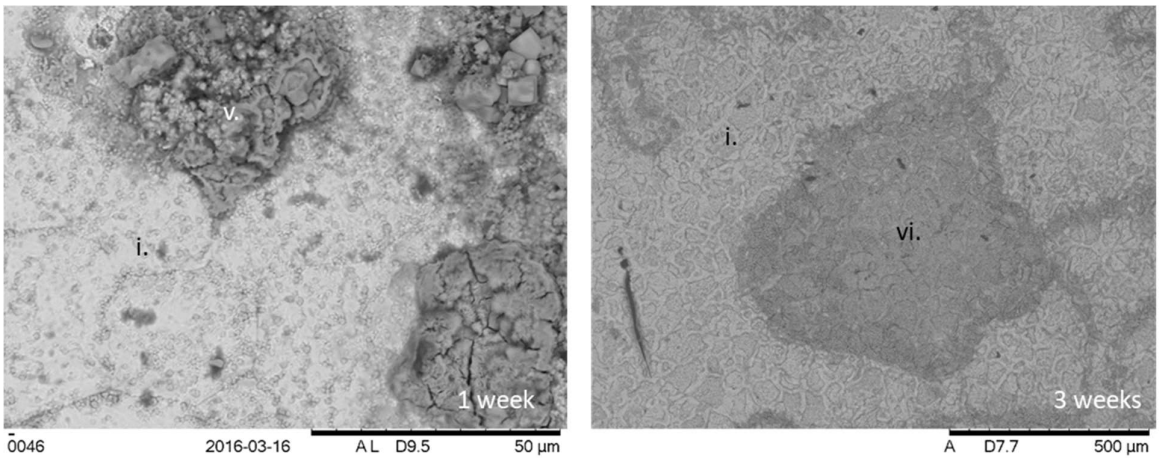

Figure 5.13: BSE images of iron held in a molten alkali chloride salt for a predetermined length of time (stated in the bottom right of each image).

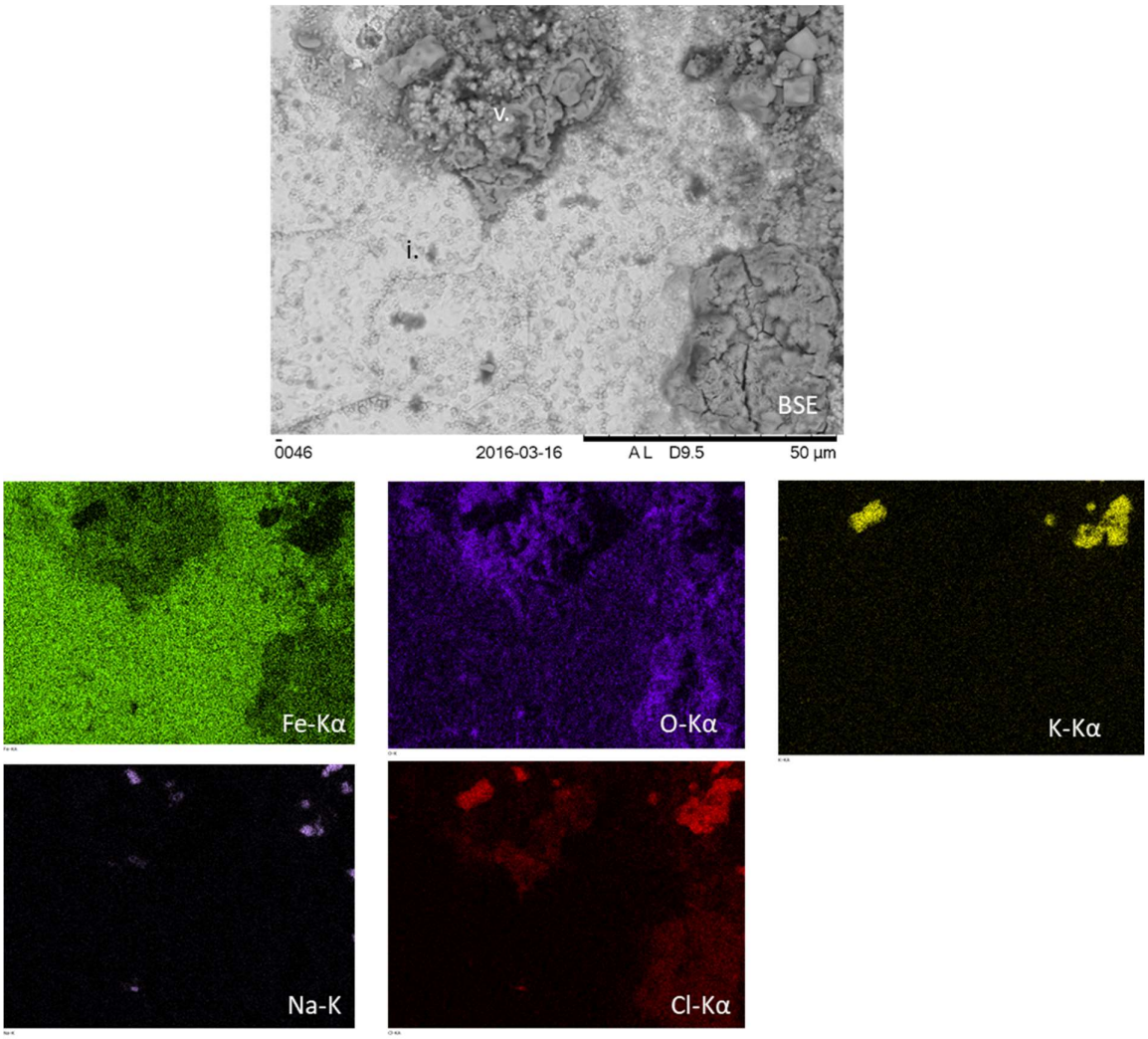

Figure 5.14: BSE image and corresponding EDX elemental maps for the surface of an iron coupon immersed in a molten alkali chloride eutectic for one week.

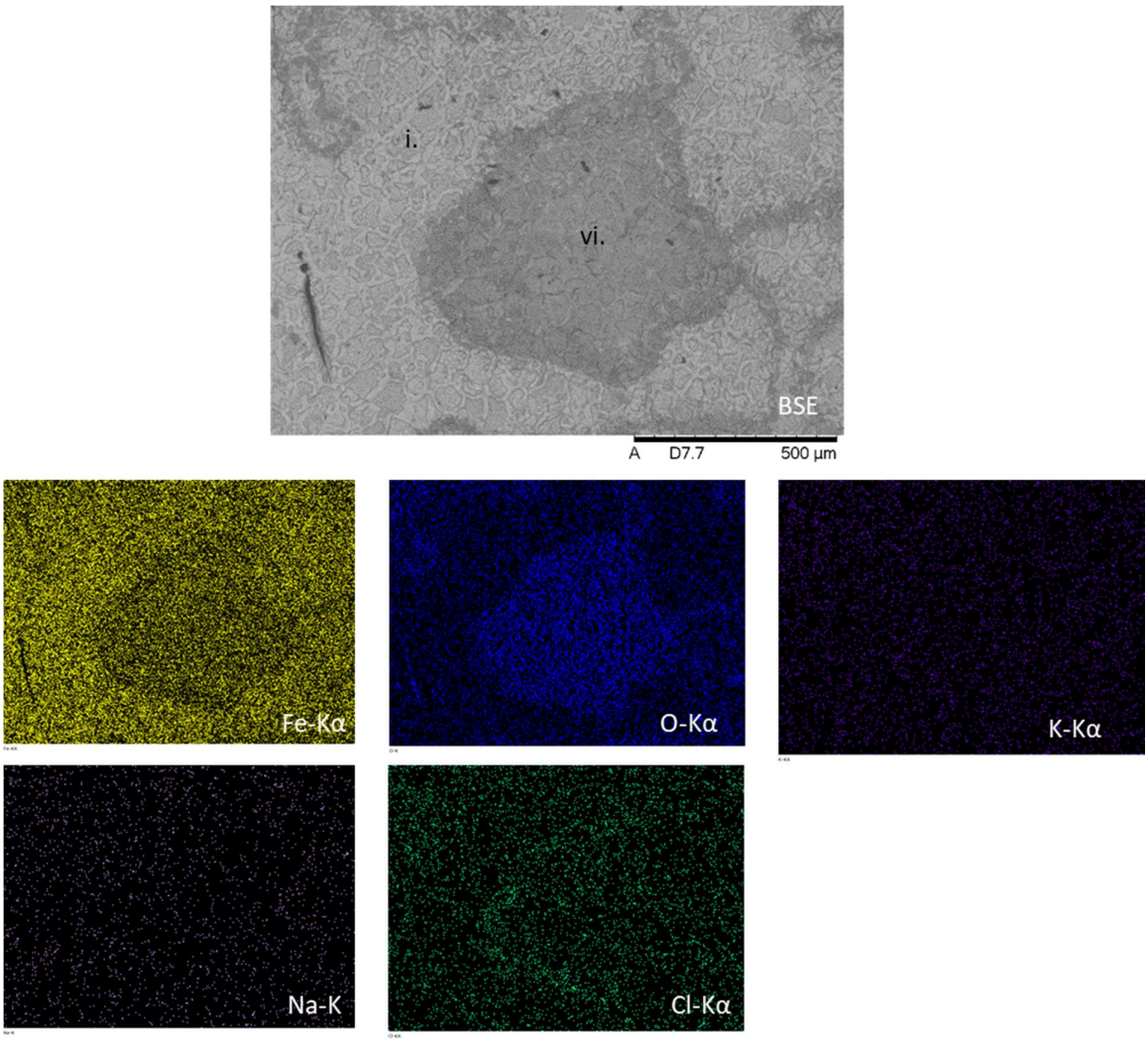

Figure 5.15: BSE image and corresponding EDX elemental maps for the surface of an iron coupon immersed in a molten alkali chloride eutectic for three weeks.

Table 5.5: Estimation of the elemental composition of the area marked as (iii) in Figure 5.14 and Figure 5.15.

Element	One week (v)	Three weeks (vi)
Iron	49.76	67.94
Oxygen	34.80	26.52
Chlorine	9.87	4.61
Carbon	5.56	0.93

The cross-sectional BSE images (Figure 5.16) obtained provide little information into the corrosion product that is formed as the corrosion product has only formed in selected areas of the surface and even after thorough investigation no clear corrosion layer was observed. Therefore, the EDX data will not be shown.

Compared to the other samples, iron has a much small array of elements, therefore the constituents that are formed are iron based compounds, namely iron oxide, which is also suggested by spot analysis. It is also possible that iron chloride is present, but this has not been confirmed with spot analysis. These results are not unexpected, but it is worth noting that considering the lack of sacrificial elements within the sample, the iron has withstood corrosion within the extreme molten salt environment exceptionally well. Iron does show a lack of surface coverage compared to the other samples and therefore it is unlikely that it will be able to withstand the extreme conditions for an extended period of time.

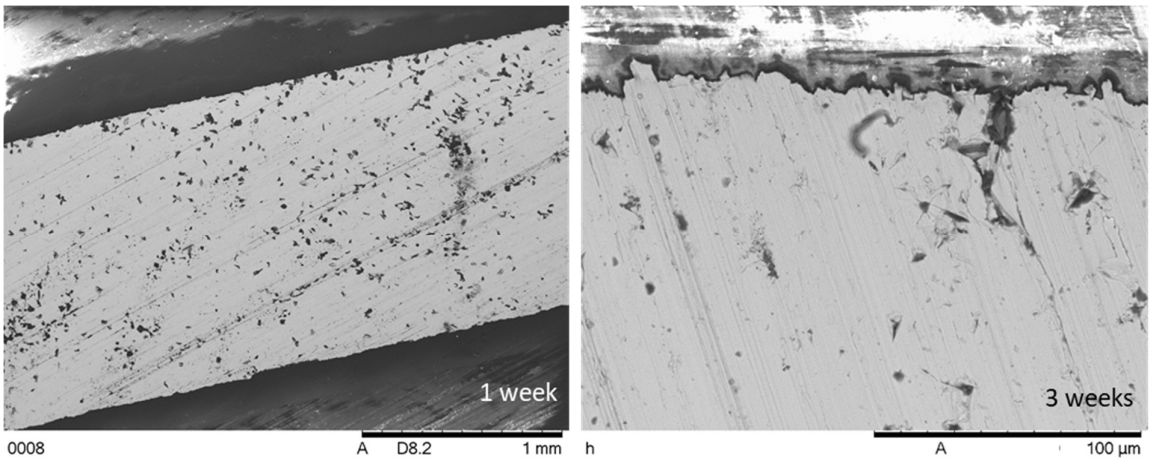

Figure 5.16: Cross sectional BSE images for iron held in a molten alkali chloride salt for a predetermined length of time (stated in the bottom right of the image).

5.4: Conclusion

In summary, the compositional tests showed that changing the elemental composition of the chromium within the system can lead to a difference in the corrosion product formed. Stainless steel 304L has a higher wt. % of chromium, but despite chromium leaching been observed, the surface coverage was significantly less compared to stainless steel 316L, suggesting that other elements may be essential to ensure a uniform corrosion layer. LDX2101 has even more chromium compared to stainless steel 304L and 316L, and although a lithium chromium oxide layer is formed it has not adhered well to the surface and a double corrosion layer has formed consisting of iron oxide, which penetrates the bulk and lithium chromium oxide. As no sacrificial elements are present within the iron bulk, it is unsurprising that iron oxide has formed, but the surprising result is how well the iron sample has withstood corrosion.

Due to the continued formation of spinels in the ternary samples, along with the odd results obtained at three weeks, the following discussion chapter will further investigate the formation of spinels in

molten chlorides, and further investigate the role of lithium, along with the anomalous results obtained at three weeks.

Literature cited

1. S. Guo, J. Zhang, W. Wu, and W. Zhou, *Corrosion in the molten fluoride and chloride salts and materials development for nuclear applications.* Progress in Materials Science, 2018. **97**: p. 448-487.
2. L. Olson, K. Sridharan, M. Anderson, and T. Allen, *Intergranular corrosion of high temperature alloys in molten fluoride salts.* Materials at High Temperatures, 2010. **27**(2): p. 145-149.
3. G. Zheng, B. Kelleher, G. Cao, M. Anderson, T. Allen, and K. Sridharan, *Corrosion of 316 stainless steel in high temperature molten Li_2BeF_4 (FLiBe) salt.* Journal of Nuclear Materials, 2015. **461**: p. 143-150.
4. I. Alvarez-Armas and S. Degallaix-Moreuil, *Duplex Stainless Steels*. 2013: John Wiley & Sons.
5. J.R. Davis, *Stainless Steels*. ASM Specialty Handbook 1999: ASM International.
6. J.H. DeVan, *Effect of Alloying Addtions on Corrosion Behavior of Nickel-Molybdenum Alloys in Fused Fluoride Mixtures (thesis)*. 1969, Oak Ridge National Laboratory
7. A.U. Malik, N.A. Siddiqi, and I.N. Andijani, *Corrosion behavior of some highly alloyed stainless steels in seawater.* Desalination, 1994. **97**(1): p. 189-197.
8. M.F. McGuire, *Stainless Steels for Design Engineers*, ed. A. International. Vol. Chapter 6. 2008.
9. J.R. Keiser, J.H. Devan, and D.L. Manning, *The corrosion resistance of type 316 stainless steel to Li_2BeF_4*. 1977, Oak Ridge National Laboratory.
10. A.R. Shankar and U.K. Mudali, *Corrosion of type 316L stainless steel in molten LiCl–KCl salt.* Materials and Corrosion, 2008. **59**(11): p. 878-882.
11. L.S. Richardson, D.C. Vreeland, and W.D. Manly, *Corrosion of Molten Fluorides.* Oak Ridge National Laboratory, 1952. **ORNL-1491**.
12. S.-H. Cho, J.-M. Hur, C.-S. Seo, and S.-W. Park, *High temperature corrosion of superalloys in a molten salt under an oxidizing atmosphere.* Journal of Alloys and Compounds, 2008. **452**(1): p. 11-15.
13. Y.Z. Yang, Y.M. Jiang, and J. Li, *In situ investigation of crevice corrosion on UNS S32101 duplex stainless steel in sodium chloride solution.* Corrosion Science, 2013. **76**: p. 163-169.